SCIENTIFIC REPORTS

OPEN

Received: 27 September 2015
Accepted: 04 November 2015
Published: 04 December 2015

Reduced GeO_2 Nanoparticles: Electronic Structure of a Nominal GeO_x Complex and Its Stability under H_2 Annealing

Jia Zhao, Linju Yang, John A. McLeod & Lijia Liu

A nominal GeO_x ($x \leq 2$) compound contains mixtures of Ge, Ge suboxides, and GeO_2, but the detailed composition and crystallinity could vary from material to material. In this study, we synthesize GeO_x nanoparticles by chemical reduction of GeO_2, and comparatively investigate the freshly prepared sample and the sample exposed to ambient conditions. Although both compounds are nominally GeO_x, they exhibit different X-ray diffraction patterns. X-ray absorption fine structure (XAFS) is utilized to analyse the detailed structure of GeO_x. We find that the two initial GeO_x compounds have entirely different compositions: the fresh GeO_x contains large amorphous Ge clusters connected by GeO_x, while after air exposure; the Ge clusters are replaced by a GeO_2-GeO_x composite. In addition, the two GeO_x products undergo different structural rearrangement under H_2 annealing, producing different intermediate phases before ultimately turning into metallic Ge. In the fresh GeO_x, the amorphous Ge remains stable, with the GeO_x being gradually reduced to Ge, leading to a final structure of crystalline Ge grains connected by GeO_x. The air-exposed GeO_x on the other hand, undergoes a $GeO_2 \rightarrow GeO_x \rightarrow Ge$ transition, in which H_2 induces the creation of oxygen vacancies at intermediate stage. A complete removal of oxides occurs at high temperature.

Ge is one of the promising candidates for anode materials in Li-ion batteries[1,2]. It has a theoretical capacity as high as 1600 mA h g^{-1} (upon formation of a $Li_{4.4}Ge$ alloy) and excellent Li^+ diffusion rate at room temperature[1]. However, the drastic volume expansion in crystalline Ge that occurs after Li insertion leads to capacity fading which limits its use in practical Li-ion devices[3]. Researchers have been seeking methods to enhance the stability of Ge anodes, such as minimizing the size of Ge[4,5], surface functionalization[2,6], morphology engineering[7,8] and forming a composite structure by coating Ge with a layer of carbon[9,10]. Recently, amorphous GeO_x ($x < 2$) structures have attracted great interest due to their ability to enhance the cycling life of Li-ion batteries[11–14]. Compared to crystalline Ge, oxidized Ge is lower cost, has better chemical stability, and improved cyclability. In fact, it has been reported that GeO_2 is able to deliver a capacity up to 2152 mA h g^{-1} if it reversibly stores 8.4 Li^+ (reactions (1) and (2))[14–16].

$$GeO_2 + 4Li \rightarrow Ge + 2Li_2O \quad (1)$$

$$Ge + 4.4Li \leftrightarrow Li_{4.4}Ge \quad (2)$$

It has been proposed that presence of Ge^0 in GeO_2 has a unique role in that it can serve as a catalyst to drive reaction (1) in the inverse direction, hence the formation of LiO_2 is reversible[17]. This catalytic

Jiangsu Key Laboratory for Carbon-Based Functional Materials & Devices, Institute of Functional Nano and Soft Materials (FUNSOM), Soochow University-Western University Center for Synchrotron Radiation Research, Soochow University, Suzhou, Jiangsu, 215123 China. Correspondence and requests for materials should be addressed to L.L. (email: ljliu@suda.edu.cn)

effect of Ge has been demonstrated by Seng *et al.* using a GeO_2/Ge/C nanocomposite as an anode for a Li battery test[17]. A nominal GeO_x structure contains a mixture of Ge dioxides and sub-oxides, as well as elemental Ge. It is critical to understand the composition and the structure of GeO_x to achieve better control of the crystallinity and grain size of the different constituents in terms of improving the battery performance.

Although there has been a large amount of work on synthesizing nanostructured GeO_x with new configurations[12,14,18], less attention has been given to understanding the starting material itself before introducing it into a battery test. GeO_x contains a mixture of Ge, GeO_x, and GeO_2, and in an oxidizing (or reducing) environment, these three components can transform from one species to another[19–21]. In fact, GeO_x has been deliberately synthesized and served either as the precursor for making Ge nanocrystals and/or GeO_2 nanostructures for the purpose of fabricating electronic and optical devices[22–24]. Although there have been relatively large amount of early studies done on Ge nanocrystal embedded GeO_x or SiO_x thin films for the purpose of electronic devices fabrication, few reports are available on the structure characterization of the free-standing Ge/GeO_x/GeO_2 nanocomposite in terms of battery applications. In particular, since amorphous Ge and GeO_x are more promising for Li-ion anodes than their crystalline counterparts, the standard crystal structure analysis tool X-ray diffraction (XRD) is no longer capable of characterizing the crystal structure of GeO_x. Transmission electron microscopy (TEM) with high resolution can tell the crystallinity of individual nanoparticles. However, for amorphous structure, distinguishing different components (e.g. Ge and GeO_x) almost entirely relies on the contrast of the image. In addition, the small sampling size of TEM lacks information on the averaged chemical composition of the material.

Aside from the crystal structure, understanding the chemical components in GeO_x from the electronic structure perspective is also important. GeO_x contains Ge in various oxidation states, from Ge^0 up to Ge^{4+}. The conventional characterization technique for studying the electronic structure of GeO_2/Ge materials is photoelectron spectroscopy[21]. This technique requires the samples to have a clean surface and be in good electrical contact with the substrate. However, nanostructured GeO_x for Li-ion battery applications are more often in the form of powder. The GeO_x therefore have irregular surfaces, which makes removing surface impurities and ensuring good electrical contact very difficult. Consequently, characterizing the electronic structure of these materials with photoelectron spectroscopy is very challenging. X-ray absorption spectroscopy, on the other hand, is an alternative tool for electronic structure characterization that is flexible in terms of sample preparation. X-ray absorption fine structure (XAFS) probes the local environment of an element of interest in the material. The spectrum originates from the interference between incoming and outgoing electrons after single and/or multiple scattering. As a result, it is a local structure probe and doesn't require the sample to be crystalline. By measuring the Ge K-edge XAFS, the chemical environment of Ge, such as its oxidation state (from the X-ray absorption near-edge structure, XANES), the coordination number, and the bond distance between Ge and the nearest neighbors (from the extended X-ray absorption fine structure, EXAFS) can be obtained[14,25–27].

GeO_x nanostructures can be synthesized using various approaches, such as hydrothermal methods[13], hydrolysis[17], and by chemical reduction[2,11]. Herein we study the electronic structure of GeO_x nanoparticles synthesized by simple chemical reduction. Such method produces GeO_x which contains GeO_2, Ge sub-oxides, and most interestingly, Ge[11]. This serves as a good starting point to investigate the electronic structure of the GeO_x, and the transitions between the three components under various conditions. We first compare the freshly prepared GeO_x, and the one stored in ambient condition for 3 days. These two samples were then used as starting materials, and were annealed in H_2 at various temperatures. The change in the chemical environment of Ge under different annealing temperatures is studied.

Results and Discussion

The freshly prepared GeO_x nanoparticles have an average size of 50 nm. Figure 1a shows a representative transmission electron microscopy (TEM) image of these particles. X-ray diffraction (XRD) measurement reveals that the fresh GeO_x and air-exposed GeO_x have very different crystal structure (Fig. 1b–d). The fresh GeO_x only contains two broad peaks, indicating its amorphous nature. The air-exposed GeO_x, on the other hand, shows well-resolved features that resemble crystalline GeO_2 with a quartz structure. After annealing in H_2 at 300 °C, the XRD patterns of both fresh GeO_x and air-exposed GeO_x are both broadened to some extent, however, the features characteristic of GeO_2 are still present in the latter. When the annealing temperature is increased to 500 °C, fresh GeO_x crystallizes into an fcc structure, with diffraction peaks matching cubic-phase metallic Ge. These features are further sharpened under annealing at 700 °C. As for air-exposed GeO_x, the 500 °C annealing results in a mixed phase containing both GeO_2 and Ge. From the intensity of the two peak series, the GeO_2 is still the major component. A full conversion from GeO_2 to Ge is observed at 700 °C annealing.

We analyse the crystalline grain size of our samples using the Scherrer equation (Eq. 3),

$$\tau = \frac{K\lambda}{\beta \cos\theta} \tag{3}$$

in which τ is the crystalline size, K is the shape factor, λ is the wavelength of the incident X-ray, β is the full width at half maximum. In this case, the values of β for 700 °C annealed fresh GeO_x and air-exposed

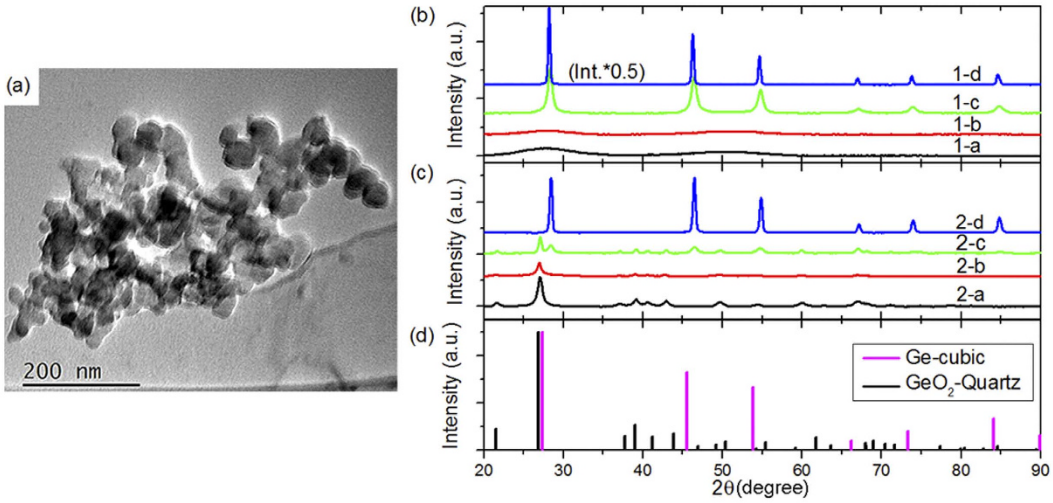

Figure 1. (**a**) TEM image of as-prepared fresh GeO_x nanoparticles. (**b**–**d**) XRD patterns of GeO_x nanoparticles before and after annealing in comparison with standards. (**b**) fresh GeO_x (sample series 1); (**c**) air-exposed GeO_x (sample series 2); (**d**) standard XRD patterns of cubic Ge and quartz GeO_2[33,34]. Labels in (**b**) and (**c**): (**a**) as-prepared samples; (**b**) samples annealed at 300 °C; (**c**) samples annealed at 500 °C; (**d**) samples annealed at 700 °C. The intensity of 1-d is reduced in half to fit the panel.

GeO_x are 0.0055 rad (0.318^0) and 0.0065 rad (0.370^0), respectively. Taking K=0.89 (the typical value of the shape factor) and $\lambda = 1.5406$ Å, we can obtain the averaged crystalline sizes for annealed fresh GeO_x and air-exposed GeO_x are 26 nm and 22 nm, respectively. The crystalline domain size of metallic Ge by annealing fresh GeO_x is slightly larger than that of air-exposed GeO_x.

Although after the final annealing, the two GeO_x possess very similar XRD patterns, the initial and intermediate phases are significantly different. Since XRD is only sensitive to structure of long-range order (i.e. crystalline), we then turn to XAFS to further examine the local structure of GeO_x nanoparticles.

Figure 2 shows the Ge K-edge XANES for all GeO_x samples, before and after annealing, in comparison with commercial GeO_2 powder. As a fully oxidized Ge standard, the XANES of GeO_2 is dominated by one sharp peak (marked by the dashed line in Fig. 2), which corresponds to the transition of an electron from the Ge 1s core level to an unoccupied 4p state. Compared to GeO_2, both GeO_x samples, with or without heat treatment, have additional features at lower energy (marked by the dotted line in Fig. 2), indicating the presence of Ge with an oxidation states lower than that in GeO_2. Recall from the XRD pattern in Fig. 1 that the fresh GeO_x is amorphous until annealed at a temperature above 500 °C. From XANES, we can see that there are both Ge- and GeO_2-like structures in the fresh GeO_x, and the lack of diffraction peaks in the XRD suggests that they are amorphous. Under annealing at 500 °C and 700 °C, crystalline Ge appears (as confirmed by XRD, refer back to Fig. 1), although there is still amorphous GeO_2 present as evidenced by XANES. On the other hand, air-exposed GeO_x is dominated by GeO_2. A slight broadening at the lower energy side of the main peak is caused by the presence of Ge sub-oxides and Ge. A sudden transition occurs after annealing at 700 °C, in which almost all the GeO_2 disappears, and the spectrum is dominated by a low-valent species Ge (spectrum 2-d). The energy onset and the spectral profile resembles the previously reported metallic Ge[2,28]. Unlike the fresh GeO_x which has a mixture of metallic Ge and amorphous GeO_2, air-exposed GeO_x after 700 °C turns almost completely to metallic Ge. We note that the XRD patterns for the fresh and air-exposed samples after annealing at 700 °C are essentially the same, but the metallic Ge-related feature in the XANES is more intense for the air-exposed sample than the fresh sample, suggesting that in the air exposed sample, a larger fraction of the available Ge is converted to cubic Ge than in the fresh sample. This is further corroborated by noting that the air-exposed sample lacks a clear GeO_2-related feature in the XANES; suggesting that so much Ge has been converted to metallic Ge that a distinct GeO_2 phase is unable to form. Recall that the air-exposed sample annealed at 700 °C exhibits a smaller grain size for metallic Ge than the fresh sample annealed at 700 °C. If any Ge oxide remaining in these samples after annealing at 700 °C occupies the space between the grains, if these grains are close-packed then the smaller grains in the air-exposed sample will lead to smaller domains of Ge oxide; possibly too small for a distinct GeO_2 lattice to form.

A closer examination of the oxidation states in Ge can be performed by examining the 1st derivative of the XANES spectra. The plots are shown in Fig. 3, and the peak positions (the edge jump) correspond to the oxidation states of Ge in the samples. This method allows us to obtain the evolution of Ge oxidation states during annealing in detail. The lower energy dashed line marks the edge jump of Ge^0 and the higher energy line marks the one of Ge^{4+}. Interestingly, the evolution of the edge jump positions as a function of annealing temperature is quite different between the two sets of GeO_x.

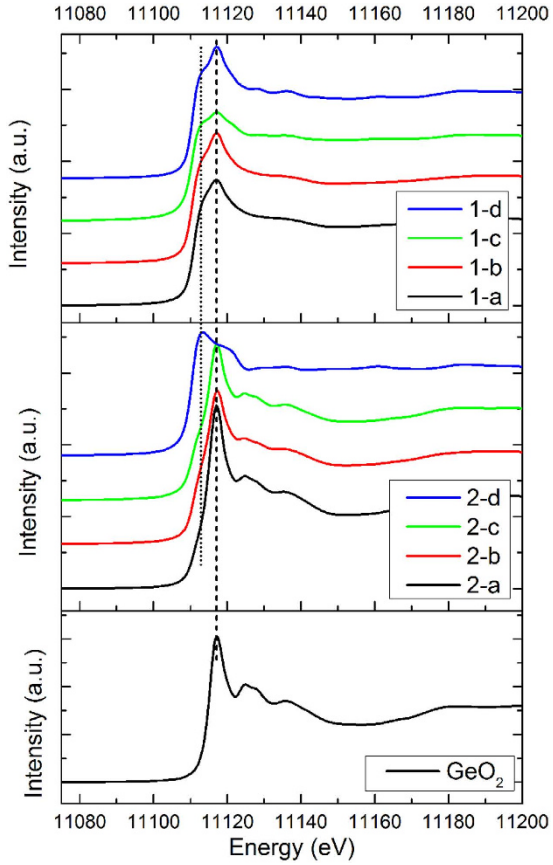

Figure 2. Ge K-edge XANES of GeO_x nanoparticles. sample series 1: fresh GeO_x, series 2: air-exposed GeO_x; (**a**) as-prepared samples, (**b**) samples annealed at 300 °C, (**c**) samples annealed at 500 °C, (**d**) samples annealed at 700 °C.

For fresh GeO_x at room temperature (spectrum 1-a in Fig. 3), the edge jump is at energy slightly higher than Ge^0, while after annealing, all the edge jumps are aligned to the position of Ge^0 regardless of temperature. Instead of Ge^0, the Ge in fresh GeO_x are slightly oxidized (i.e. $0 < x \leq 2$). After annealing at 300 °C, GeO_x undergoes a disproportionation reaction, producing Ge and GeO_2 (reaction (4)), leading to the lower-energy shift of the main peak position, and a better-defined GeO_2 edge jump.

$$2GeOx \rightarrow (2 - x)\,Ge + xGeO_2 \tag{4}$$

The disproportionation reaction of GeO_x into Ge and GeO_2 is commonly observed in Ge nanostructure synthesis. The reaction takes place when GeO_x is annealed in a non-oxidizing environment, and is considered as one of the intermediate stages in forming a Ge-GeO_2 complex[22]. It has been observed experimentally using XANES that annealing GeO_x thin films under N_2 results in a low-energy shift in the shoulder feature and an intensity increase in GeO_2 feature[27,29]. At 500 °C annealing, the GeO_2 decreases noticeably, while Ge remains almost unchanged. At this temperature, the reduction of GeO_x starts to take place and O is being removed out of the system. The amorphous Ge clusters starts to crystalize. At 700 °C, phase separation takes place, Ge forms large crystalline grains and the left over GeO_2 migrates to the grain boundary.

As for air-exposed GeO_x, the one at room temperature contains both fully oxidized GeO_2 and Ge sub-oxide. The Ge sub-oxide component exhibit a progressive shift at alleviated annealing temperature until it becomes Ge^0, while the edge jump of the GeO_2 component remains stable but the intensity decrease until it totally disappears as the temperature reaches 700 °C.

The results above demonstrate that the fresh GeO_x and air-exposed GeO_x has distinct compositions, and because of this, they undergo different crystallization processes under H_2 annealing, even though the ultimate products have identical XRD patterns. The fresh GeO_x is always a mixture of Ge and GeO_2, while air-exposed GeO_x is dominated by GeO_2 at low and intermediate temperatures with a gradual emergence of Ge, and GeO_2 is fully converted to Ge^0 at high annealing temperature.

The Fourier transformed EXAFS spectra of GeO_x are shown in Fig. 4. The amplitude was fitted using the IFFEFIT package at the R-range between 1.0 Å and 2.5Å (first shell). Detailed structural parameters,

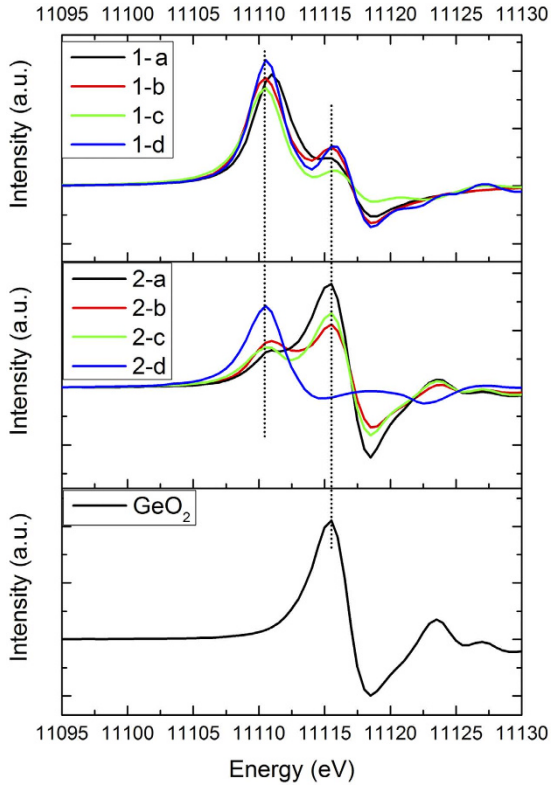

Figure 3. Ge K-edge XANES of GeO_x nanoparticles plotted in 1st derivatives. The legend is the same as the one shown in Fig. 2.

such as the Ge coordination number (CN), Ge-O and Ge-Ge bond distance (R), Debye Waller factor (σ^2), and inner potential shift (ΔE) are listed in Table 1.

It can be clearly seen from Fig. 4 that the fresh GeO_x contains significant amount of Ge-Ge bonding, with bond distance of ~2.45Å. This bond length is consistent with previous EXAFS studies of Ge-Ge bonding[30]. The $CN_{Ge\text{-}Ge}$ is less than the one of metallic Ge, indicating its amorphous nature. As for the oxide component, Ge-O bonds are present in the material with bond lengths close to that of GeO_2. Compared to GeO_2, only the first shell Ge-O is present in GeO_x; the features from second shell (features around 2.5Å to 3.2Å) are missing. The low $CN_{Ge\text{-}O}$ means GeO_x are highly under-coordinated compared to GeO_2.This further confirms that the GeO_x components in the fresh samples lack long range order. The as-prepared GeO_x contains both GeO_x and Ge clusters in an amorphous form.

Under annealing at 300 °C, the $CN_{Ge\text{-}O}$ remains almost unchanged (within the error range), while the $CN_{Ge\text{-}Ge}$ increases. The values deduced from the fitting further supports our proposed reaction of GeO_x disproportionation at 300 °C (reaction 4). During the reaction, O atom is transferred from one Ge to another Ge, leaving one Ge with dangling bond, and then two adjacent Ge joined together to form Ge-Ge bond. A similar reaction scheme was proposed by Wang *et al.* on vacuum annealed GeO film[21], and our result is consistent with their observation.

The Ge-O bond almost disappears after annealing at 500 °C, while there is a slight decrease in $CN_{Ge\text{-}Ge}$. At this stage, reduction of GeO_x (reaction (5)) becomes the dominant reaction in the system. This reaction leads to the consumption of GeO_x, hence a significant decrease of $CN_{Ge\text{-}O}$.

$$GeO_x + xH_2 \rightarrow Ge + xH_2O \ (x \leq 1) \quad (5)$$

As the temperature further increases, thermal induced crystallization takes place, the Ge clusters becomes highly coordinated, with $CN_{Ge\text{-}Ge}$ approaches metallic Ge.

We should note that $CN_{Ge\text{-}Ge}$, $CN_{Ge\text{-}O}$, and the intensity of the XANES features are smaller for the sample annealed at 500 °C than for the other samples (refer back to Fig. 2 and Table 1). There are two possible explanations for this: One is that at 500 °C disproportionation into cubic Ge and amorphous GeO_2 is complete, but these phases exist as finely mixed nanoscale domains (this is supported by the rather broad XRD pattern of cubic Ge from the sample annealed at 500 °C, refer back to Fig. 1(b)). These very small domains indicate a relatively large amorphous boundary region, in which the general lack of structure would lead to a more intense background in the XAFS spectrum that reduces the relative amplitude of the fine structure features related to the Ge and GeO_2 and phases. After annealing at 700 °C

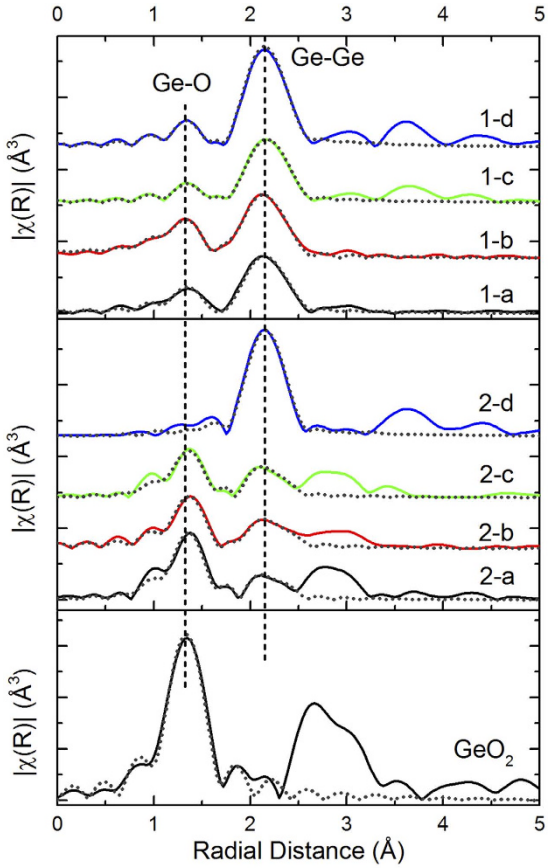

Figure 4. Fourier transforms of Ge K-edge k^3-weighted EXAFS data in R-space with first-shell fits. Solid lines: experimental spectra; dotted lines: fitted spectra. Sample series 1: fresh GeO_x, series 2: air-exposed GeO_x. The labels are the same as the ones in Fig. 2.

Name	Temperature	Shell	CN	R(Å)	ΔE (eV)	σ^2 (10^{-3} Å^2)	R-factor
GeO2	RT	Ge-O	4	1.74(0.01)	6.33	1.4(1.0)	0.011
Fresh GeO_x	RT	Ge-O	1.5(0.2)	1.76(0.01)	8.10	4.2(2.0)	0.006
		Ge-Ge	2.3(0.3)	2.45(0.01)	7.62	4.6(0.8)	
	300	Ge-O	1.3(0.1)	1.74(0.01)	6.88	2.9(1.1)	0.002
		Ge-Ge	2.8(0.2)	2.46(0.005)	7.74	5.4(0.5)	
	500	Ge-O	0.7(0.1)	1.73(0.01)	6.44	1.6(1.7)	0.003
		Ge-Ge	2.4(0.2)	2.46(0.005)	8.97	4.4(0.5)	
	700	Ge-O	1.1(0.2)	1.73(0.02)	7.19	3.2(2.4)	0.007
		Ge-Ge	3.5(0.8)	2.45(0.01)	6.33	4.2(1.5)	
Air-exposed GeO_x	RT	Ge-O	3.3(0.3)	1.74(0.01)	-3.21	1.9(0.9)	0.011
		Ge-Ge	0.5(0.3)	2.48(0.01)	8.00	1.2(3.1)	
	300	Ge-O	2.5(0.2)	1.75(0.01)	-3.22	2.6(1.2)	0.004
		Ge-Ge	0.9(0.4)	2.46(0.03)	9.91	3.0(2.8)	
	500	Ge-O	2.2(0.2)	1.74(0.01)	-3.02	2.4(1.4)	0.014
		Ge-Ge	0.7(0.3)	2.46(0.02)	6.27	1.7(2.6)	
	700	Ge-O	0.2(0.1)	1.69(0.04)	-3.2	1.0(0.8)	0.010
		Ge-Ge	4.1(0.3)	2.45(0.002)	6.47	4.0(0.5)	

Table 1. EXAFS fitting parameters for GeO_x nanoparticles.

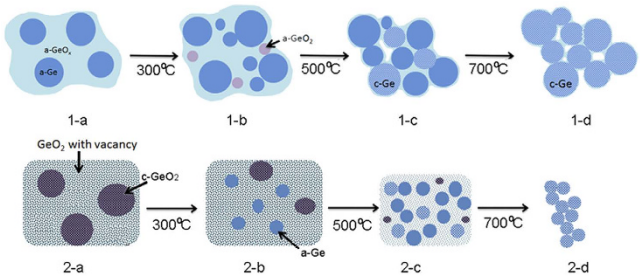

Figure 5. Illustration of the structure of GeO_x nanoparticles, fresh (1-a) and air-exposed (2-a), and their compositions under H_2 annealing. The labels are the same as the ones in Fig. 2.

the respective cubic Ge and amorphous GeO_2 domains are large enough to be resolved separated in the XAFS spectrum. On the other hand, it is possible that the pellet prepared from the 500 °C sample was slightly too thick for XAFS and consequently the XANES features and coordination numbers are reduced by the "thickness effect"[31]. We would like to stress that the ratio of $CN_{Ge\text{-}O}$ to $CN_{Ge\text{-}Ge}$ is the same for the samples annealed at 500 °C and 700 °C (~0.3), and both are lower than those for the samples annealed at 300 °C (0.46) and as-prepared (0.65). The thickness of the XAFS sample would affect $CN_{Ge\text{-}O}$ and $CN_{Ge\text{-}Ge}$ equally, so this observation is independent of possible measurement artefacts. Therefore regardless of whether the anomalous aspects of the XANES and EXAFS from the sample annealed at 500 °C are due to nanoscale GeO_2, Ge phase separation, or are due to a measurement artefact, the discussion above shows that the disproportionation reaction (4) is largely complete after annealing at 500 °C, and that higher temperatures simply improve phase separation and growth of larger crystals of Ge. We should also point out that a previous report shows that high temperature (above 500 °C) annealing induces the crystallization of GeO_x[23], which would lead to O migration to the edges of the cubic Ge domains. This could also lead to the increase in the $CN_{Ge\text{-}O}$ from the sample annealed at 500 °C to the one annealed at 700 °C.

As for the air-exposed GeO_x, the material retains GeO_2-like features from room temperature up to 500 °C. The room temperature sample contains mostly undercoordinated GeO_2, and the $CN_{Ge\text{-}O}$ is much closer to GeO_2 compared to fresh GeO_x. The second shell component of radial distance above 2.4Å is also present, so that air-exposed GeO_x is more of a GeO_2-like crystalline structure. This also explains why GeO_2-like pattern only appears in the XRD of air-exposed GeO_x but not the fresh ones. Small amounts of Ge-Ge bonds are present in the sample too, but from their low CN and long Ge-Ge distance, they are unlikely to be Ge clusters. Instead, the system is more like GeO_2 with oxygen vacancies, in which Ge is present as dangling bonds.

Unlike fresh GeO_x, the disproportionation reaction does not happen in the air-exposed GeO_x sample system. From Table 1, we see a decrease in $CN_{Ge\text{-}O}$, while $CN_{Ge\text{-}Ge}$ remains almost constant at 300 °C. Annealing the GeO_x in a reduced environment only partially removes O atoms (i.e. amorphorization), following the reaction (6), which produces a highly oxygen-deficient GeO_2 structure. Meanwhile, the Ge-Ge distance gets shorter, indicating the formation of amorphous Ge cluster.

$$GeO_x + yH_2 \rightarrow GeO_{x-y} + yH_2O \ (1 \leq x \leq 2,\ y < x) \tag{6}$$

At 500 °C, the decrease of $CN_{Ge\text{-}O}$ slows down. Recall from Fig. 1, metallic Ge features start to appear in the XRD, so at this stage, structural rearrangement start to occur. Note the Ge-O long-range order also improves as seen in Fig. 4. A system with many oxygen vacancies is not thermodynamically stable, so O migrates, and produces GeO_2 and adjacent Ge start to join each other forming Ge-Ge bonds. At 700 °C, the high temperature leads to a total reduction of GeO_x (reaction (7)), leading to a sudden transition from GeO_x to Ge. Upon the removal of almost all O in GeO_x, the Ge grows into cubic crystallites. The relative rapidity of this transition may explain why these crystallites are somewhat smaller than those that form during the more gradual crystallization during annealing in the fresh GeO_x samples. As the O is almost all removed, a distinct GeO_x phase no longer exists. This is evidenced by the lack of a clear GeO2-related feature in the XANES spectrum from the air-exposed sample annealed at 700 °C (refer back to Fig. 2), as well as the anomalously short Ge-O bond length obtained from EXAFS fitting (see Table 1). The remaining O is likely only found as a capping layer on the Ge crystallites.

$$GeO_x + xH_2 \rightarrow Ge + xH_2O \ (1 \leq x \leq 2) \tag{7}$$

The structures of the two GeO_x samples and their behaviour under H_2 annealing can be summarized in the scheme shown in Fig. 5. The fresh GeO_x contains both elemental Ge and GeO_x (x closes to 1), both are amorphous and present in comparable amounts. H_2 annealing induces the disproportionation and reduction of GeO_x, forming more Ge clusters. Ge clusters crystalize at high annealing temperatures, and grain boundaries are filled with GeO_x. Air-exposed GeO_x, on the other hand, can be modelled as GeO_2 crystallites with O vacancies. Ambient air introduces oxygen, and the initial product is mostly

crystalline GeO_2 with GeO_x where x closes to 2. H_2 annealing gradually creates more oxygen vacancies, reducing the presence of crystalline GeO_2 and leading to the formation of more Ge dangling bonds. The GeO_x structure is completely eliminated at the temperature of 700 °C, when a transition to crystalline Ge occurs due to the H_2 reduction reaction.

Conclusion

As nominal GeO_x compounds, the actual compositions could vary significantly from material to material, depending on the synthesis strategies and post-treatment conditions. We have demonstrated that the exact composition and structure of GeO_x and its structural evolution during annealing can be successfully analyzed using XAFS. In our model system, GeO_x nanoparticles were synthesized by chemical reduction of GeO_2, freshly prepared GeO_x is found consisting of Ge clusters and GeO_x (x closes to 1), both in amorphous forms. Such GeO_x undergoes disproportionation when annealed in a reducing environment. The amount of amorphous Ge increases, and finally crystallizes into metallic Ge, with GeO_x presents at the grain boundaries. However, if the GeO_x is exposed to ambient conditions, the elemental Ge domains are quickly replaced by oxides, and the nanoparticles turn into a GeO_2-like structure. Once such structure formed, the GeO_x (x closes to 2) can be slowly reduced by H_2, under mild temperature, producing small Ge crystallites embedded in GeO_x matrix. Once the temperature reaches 700 °C, there is a complete conversion of GeO_x to Ge. The composition of GeO_x can change significantly from its initial composition after exposure to oxygen, and this exposure also affects how the structural rearrangement takes place during post-treatment. These findings are of paramount importance to developing GeO_x anodes for Li-ion batteries. In particular, they highlight the importance of carefully controlled synthesis of GeO_x anodes – as even under identical preparation conditions, the composition and crystal structure can completely change based on whether or not the samples are exposed to ambient conditions. A controlled regime of air exposure followed by annealing in H_2 can further tailor the composition of the material. All the samples investigated here have nominal GeO_x structures, but each of them possesses unique structures, which are identified by XAFS. With this in mind, the next step of the research includes the examination of Li battery performance with integration of these materials. The device performance can then be related to the fundamental structures of the GeO_x. Amorphous Ge is preferable to crystalline Ge for Li-storage, but smaller clusters are also preferable to larger clusters. If the composition of the GeO_x is tunable, we will be able to find which configuration is desired as an anode material.

Methods

Material Synthesis. GeO_x nanoparticles were prepared using a chemical reduction method[11,24]. 2.0 g of GeO_2 (99.99%, Aladdin) was first dissolved in 36 mL deionized water, and 7 mL of NH_4OH (28%-30% NH_3, Aladdin) was added. Freshly prepared $NaBH_4$ (98%, Aladdin) solution (3.616 g in 20 mL deionized water) was quickly added to the mixture. The solution was vigorously stirred for 20h at room temperature. The resulting product was then filtered, washed with deionized water, and dried under vacuum at 50 °C. The freshly prepared GeO_x was divided into two parts, one sealed in a glass vial and kept in a glove box filled with N_2 (denoted as fresh GeO_x), and the other one was kept in a desiccator (humidity $<3\%$) for 3 days (denoted as air-exposed GeO_x). H_2 annealing was conducted in a tube furnace. GeO_x was placed in a combustion crucible at the centre of the tube, and 2% H_2 was introduced to the tube at a rate of 50 sccm (standard-state cubic centimetre per minute). The samples were annealed at 300 °C, 500 °C and 700 °C, respectively, under the H_2 flow. The temperature was increased at a rate of 2.1 °C/min, and held at the desired temperature for 30 min. After annealing, the samples were cooled down to the room temperature.

Characterization. X-ray diffraction (XRD) and transmission electron microscopy (TEM) characterization was performed at the Institute of Functional Nano and Soft Materials (FUNSOM), Soochow University. XRD was done using a PANalytical (Empyrean) apparatus with Cu Kα as the probing source. The morphology of the as-prepared GeO_x was examined using TEM (Tecnai G2 F20, FEI). The Ge K-edge XAFS experiments were conducted at beamlines BL01C1 at National Synchrotron Radiation Research Center (NSRRC), Taiwan and BL12B1 at SPring8, Japan. NSRRC is a 1.5 GeV storage ring operating at the beam current of 360 mA in top-up mode. The beamline, BL01C1 has energy range of 6–33 keV and a resolution $\Delta E/E$ of 2.3×10^{-4}. SPring-8 is an 8 GeV ring operating at the beam current of 100 mA in top-up mode. BL12B1 has an energy range of 5–25 keV with resolution $\Delta E/E$ of 10^{-4}. The GeO_x powder was pressed into thin pellets and sealed in Kapton tape. The spectra were measured using transmission mode. Commercially obtained GeO_2 powder (99.99%, Aladdin) was used as a reference.

XAFS data analysis. XAFS data was processed following the standard procedure using the IFFEFIT software package[32]. Briefly, in the pre-edge region, the spectrum was fitted to a straight line, and the post-edge background was fitted with a cubic spline. The EXAFS function, χ, was obtained by subtracting the post-edge background from the overall absorption and then normalizing with respect to the edge jump step. The EXAFS fitting was performed in *R*-space between 1.0 Å and 2.6 Å (the Fourier transform from *k*-space was performed over a range of 3.0 to 14.0 $Å^{-1}$), taking both Ge-O and Ge-Ge shells into consideration. The amplitude reduction factor S_0^2 was determined to be 0.85 ($\pm$0.09), using GeO_2 powder of quartz-phase and assuming Ge is fully coordinated with a coordination number (CN) of 4. Structural

parameters of the GeO_x samples, such as coordination numbers, bond distance (R), Debye-Waller factor (σ^2), and inner potential shift (E_0) were fitted using the IFEFFIT code.

References

1. Graetz, J., Ahn, C. C., Yazami, R. & Flultz, B. Nanocrystalline and thin film germanium electrodes with high lithium capacity and high rate capabilities. *J. Electrochem. Soc.* **151,** A698–A702, (2004).
2. Lee, H. *et al.* Surface-stabilized amorphous germanium nanoparticles for lithium-storage material. *J. Phys. Chem. B* **109,** 20719–20723, (2005).
3. Kim, M. G. & Cho, J. Nanocomposite of amorphous Ge and Sn nanoparticles as an anode material for Li secondary battery. *J. Electrochem. Soc.* **156,** A277–A282, (2009).
4. Lee, H., Kim, H., Doo, S.-G. & Cho, J. Synthesis and optimization of nanoparticle Ge confined in a carbon matrix for lithium battery anode material. *J. Electrochem. Soc.* **154,** A343–A346, (2007).
5. Kennedy, T. *et al.* High-performance germanium nanowire-based lithium-ion battery anodes extending over 1000 cycles through *in situ* formation of a continuous porous network. *Nano Lett.* **14,** 716–723, (2014).
6. Park, M. H., Kim, K., Kim, J. & Cho, J. Flexible dimensional control of high-capacity Li-ion-battery anodes: from 0D hollow to 3D porous germanium nanoparticle assemblies. *Adv. Mater.* **22,** 415–418, (2010).
7. Park, M. H. *et al.* Germanium nanotubes prepared by using the Kirkendall effect as anodes for high-rate lithium batteries. *Angew. Chem. Int. Ed.* **50,** 9647–9650, (2011).
8. Xue, D. J. *et al.* Improving the electrode performance of Ge through Ge@C core-shell nanoparticles and graphene networks. *J. Am. Chem. Soc.* **134,** 2512–2515, (2012).
9. Cui, G. *et al.* A germanium-carbon nanocomposite material for lithium batteries. *Adv. Mater.* **20,** 3079–3083, (2008).
10. Wang, X. L. *et al.* Amorphous hierarchical porous GeO_x as high-capacity anodes for Li ion batteries with very long cycling life. *J. Am. Chem. Soc.* **133,** 20692–20695, (2011).
11. Choi, S. H., Jung, K. Y. & Kang, Y. C. Amorphous GeO_x-coated reduced graphene oxide balls with sandwich structure for long-life lithium-ion batteries. *ACS Appl. Mater. Interfaces* **7,** 13952–13959, (2015).
12. Lin, Y.-M., Klavetter, K. C., Heller, A. & Mullins, C. B. Storage of lithium in hydrothermally synthesized GeO_2 nanoparticles. *J. Phys. Chem. Lett.* **4,** 999–1004, (2013).
13. Hwang, J. *et al.* Mesoporous Ge/GeO_2/carbon lithium-ion battery anodes with high capacity and high reversibility. *ACS Nano* **9,** 5299–5309, (2015).
14. Pena, J. S. *et al.* Electrochemical reaction between lithium and β-quartz GeO_2. *Electrochem. Solid-State Lett.* **7,** A278–A281, (2004).
15. Feng, J. K., Lai, M. O. & Lu, L. Influence of grain size on lithium storage performance of germanium oxide films. *Electrochimica Acta* **62,** 103–108, (2012).
16. Seng, K. H., Park, M. H., Guo, Z. P., Liu, H. K. & Cho, J. Catalytic role of Ge in highly reversible GeO_2/Ge/C nanocomposite anode material for lithium batteries. *Nano Lett.* **13,** 1230–1236, (2013).
17. Fang, Z. *et al.* 3D hollow framework of GeO_x with ultrathin shell for improved anode performance in lithium-ion batteries. *Electrochimica Acta* **151,** 453–458, (2015).
18. Wu, J. *et al. In situ* structural evolution from GeO nanospheres to GeO/(Ge, GeO_2) core-shell nanospheres and to Ge hollow nanospheres. *CrystEngComm* **13,** 4611, (2011).
19. Shinde, S. L. & Nanda, K. K. Thermal oxidation strategy for the synthesis of phase-controlled GeO_2 and photoluminescence characterization. *CrystEngComm* **15,** 1043–1046, (2013).
20. Wang, S. K., Liu, H.-G. & Toriumi, A. Kinetic study of GeO disproportionation into a GeO_2/Ge system using x-ray photoelectron spectroscopy. *Appl. Phys. Lett.* **101,** 061907, (2012).
21. Zhang, Y. F. *et al.* Germanium nanowires sheathed with an oxide layer. *Phys. Rev. B* **61,** 4518–4521, (2000).
22. Vijayarangamuthu, K. *et al.* Ge nanocrystals embedded in a GeO_x matrix formed by thermally annealing of Ge oxide films. *J. Vac. Sci. Technol. A* **27,** 731, (2009).
23. Jing, C., Zang, X., Bai, W., Chu, J. & Liu, A. Aqueous germanate ion solution promoted synthesis of worm-like crystallized Ge nanostructures under ambient conditions. *Nanotechnology* **20,** 505607, (2009).
24. Peng, M. *et al.* Electronic structure and photoluminescence origin of single-crystalline germanium oxide nanowires with green light emission. *J. Phys. Chem. C* **115,** 11420–11426, (2011).
25. Ridgway, M. C. *et al.* EXAFS characterisation of Ge nanocrystals in silica. *Nucl. Instrum. Meth. Phys. Res. B* **218,** 421–426, (2004).
26. Sahle, C. J. *et al.* Phase separation and nanocrystal formation in GeO. *Appl. Phys. Lett.* **95,** 021910, (2009).
27. Ge XRD pattern from ICSD (ICDD 01-089-4164), from Smakula, A. & Kalnajs, J. Precision Determination of Lattice Constants with a Geiger-Counter X-ray Diffractometer. *Phys. Rev.* **99,** 1737, (1955).
28. Schacht, A. *et al.* Temperature-induced obliteration of sub-oxide interfaces in amorphous GeO. *J. Non-Crystalline Solids* **355,** 1285–1287, (2009).
29. Little, W. *et al.* Structural origin of light emission in germanium quantum dots. *Scientific Reports* **4,** 7372, (2014).
30. Stern, E. A. & Kim, K. Thickness effect on the extended-x-ray-absorption-fine-structure amplitude. *Phys. Rev. B*, **23,** 3781–3787, (1981).
31. Yuan, F.-W., Yang, H.-J. & Tuan, H.-Y. Alkanethiol-passivated Ge nanowires as high-performance anode materials for lithium-ion batteries: the rold of chemical surface functionalization. *ACS Nano* **6,** 9932–9942, (2012).
32. Newville, M. IFEFFIT: interactive EXAFS analysis and FEFF fitting. *J. Synchrotron Rad.* **8,** 322–324, (2001).
33. GeO2 XRD pattern from ICSD (ICDD 01-083-2476), from Jorgensen, J. D., Compression mechanisms in α-quartz structures – SiO_2 and GeO_2. *J. Appl. Phys.* **49,** 5473, (1978).
34. Gerion, D. *et al.* Solution synthesis of germanium nanocrystals: success and open challenges. *Nano Lett.* **4,** 597–602, (2004).

Acknowledgements

This work is funded by National Natural Science Foundation of China (NSFC) (project numbers 21403147, 11404232, and U1432106). The authors acknowledge the support from Soochow University-Western University Center for Synchrotron Radiation Research and Collaborative Innovation Center of Suzhou Nano Science and Technology (NANO-CIC), Soochow University. J. Z. acknowledges the help from Mr. Mo Sha for the H_2 annealing experiment.

Author Contributions

L.L. conceived and designed the experiments. J.Z. synthesized GeO_x nanoparticles and performed the preliminary characterization. L.Y. and J.Z. conducted the XAFS measurements. J.A.M. and L.L. performed the spectra analysis and wrote the manuscript. All authors discussed and commented on the manuscript.

Additional Information

Competing financial interests: The authors declare no competing financial interests.

How to cite this article: Zhao, J. *et al.* Reduced GeO_2 Nanoparticles: Electronic Structure of a Nominal GeO_x Complex and Its Stability under H_2 Annealing. *Sci. Rep.* **5**, 17779; doi: 10.1038/srep17779 (2015).

This work is licensed under a Creative Commons Attribution 4.0 International License. The images or other third party material in this article are included in the article's Creative Commons license, unless indicated otherwise in the credit line; if the material is not included under the Creative Commons license, users will need to obtain permission from the license holder to reproduce the material. To view a copy of this license, visit http://creativecommons.org/licenses/by/4.0/